8-1-1993

Gravity Wave-Driven Fluctuations in the O2 Atmospheric (0-1) Nightglow from an Extended, Dissipative Emission Region

Michael P. Hickey Ph.D.
Embry-Riddle Aeronautical University, hicke0b5@erau.edu

G. Schubert
University of California - Los Angeles

R. L. Walterscheid
The Aerospace Corporation

Scholarly Commons Citation

Hickey, M. P., G. Schubert, and R. L. Walterscheid (1993), Gravity wave-driven fluctuations in the O2 atmospheric (0-1) nightglow from an extended, dissipative emission region, J. Geophys. Res., 98(A8), 13717–13729, doi: https://doi.org/10.1029/92JA02348.

JOURNAL OF GEOPHYSICAL RESEARCH, VOL. 98, NO. A8, PAGES 13,717–13,729, AUGUST 1, 1993

Gravity Wave-Driven Fluctuations in the O_2 Atmospheric (0-1) Nightglow from an Extended, Dissipative Emission Region

MICHAEL P. HICKEY

Physitron, Inc., Huntsville, Alabama

G. SCHUBERT

Department of Earth and Space Sciences and Institute of Geophysics and Planetary Physics University of California, Los Angeles

R. L. WALTERSCHEID

Space and Environment Technology Center, The Aerospace Corporation, Los Angeles

The omission fluctuations of the O_2 atmospheric $\left(O_2\left(b^1\Sigma_g^+\right)\right)$ nightglow due to gravity waves, evanescent waves, and acoustic waves are calculated using the Eulerian model formalism of Schubert et al. (1991) from which the complex parameter $<\eta>$ is derived: $\langle\eta\rangle=\left(\langle I'\rangle/\langle\bar{I}\rangle\right)/\left(\langle T_I'\rangle/\langle\bar{T}_I\rangle\right)$ where I is the nightglow intensity, T_I is intensity-weighted temperature, the brackets denote an altitude integration over all emitting layers, an overbar denotes an unperturbed state and a prime denotes a perturbation about the unperturbed state. The $\left(O_2\left(b^1\Sigma_g^+\right)\right)$ state is assumed to form directly by the three-body association reaction involving atomic oxygen $\left(O+O+M->O_2\left(b^1\Sigma_g^+\right)+M\right)$ and also via quenching of the intermediate state $O_2\left(c^1\Sigma_u^-\right)$. Our calculated values of $<\eta>$ are compared with those derived from the observations of Zhang (1991) and Zhang et al. (1992a). These observations, which were obtained during the AIDA (Arecibo Initiative in Dynamics of the Atmosphere) Act '89 campaign at Arecibo (18°N) during the period covering April 5 to May 9, 1989, were made with the MORTI (mesopause oxygen rotational temperature imager) instrument and provide us with values of both $<\eta>$ and the horizontal wavelengths of the gravity waves. For all of our results the undisturbed mesosphere is defined by the model output of Garcia and Solomon (1985) for a latitude of 18° and for the months of March and June, these being most relevant to the observations of Zhang. For the evanescent waves, there is essentially good agreement between the theory and observations, while for the internal waves the agreement is best for $|<\eta>|$. However, the comparatively larger errors in the observed values of $|<\eta>|$ make it impossible to decide which chemical scheme used in the model provides the best results. The errors associated with the observed phases of $<\eta>$ are apparently minimal, and cannot account for the differences between the observed and modeled phases of $<\eta>$. The sensitivity of our modeled values of $<\eta>$ to certain rate constants and the quenching parameters is investigated and discussed. In particular, we demonstrate that our modeled values of $<\eta>$ are sensitive to the quenching effects of atomic oxygen and hence also to the production mechanism of the $\left(O_2\left(b^1\Sigma_g^+\right)\right)$.

Introduction

The modeling of the effects of gravity waves on various nightglow emissions has made significant progress in the last few years, and has totally superseded the original theoretical treatment of *Krassovsky* [1972]. In that study, Krassovsky's observations of the OH nightglow modulations were interpreted in terms of a parameter η, the instantaneous ratio of relative brightness oscillations to relative temperature oscillations. It is now well understood that η is a complex quantity [*Walterscheid et al.*, 1987] that must be calculated by including contributions from every altitude of the emission layer [*Hines and Tarasick*, 1987; *Schubert and Walterscheid*, 1988]. Furthermore, at long wave periods it is essential that the effects of eddy diffusivities be incorporated into the gravity wave dynamics [*Hickey*, 1988a, b; *Schubert et al.*, 1991]. Other recent studies of wave-induced fluctuations in nightglow emissions include those of *Walterscheid and Schubert* [1987, 1989], *Tarasick and Hines* [1990], *Tarasick and Shepherd* [1992a, b], *Hickey et al.* [1992], and *Zhang et al.* [1992b].

In our previous studies of the interaction between gravity waves and the airglow, we concentrated on the OH Meinel nightglow. Here, we apply our model to the O_2 atmospheric (0-1) band nightglow. The chemistry relevant to the O_2 atmospheric nightglow is far less understood than that of the OH Meinel, and much controversy exists regarding the excitation mechanism involved in the production of the O_2 atmospheric precursor state [e.g., *Stegman and Murtagh*, 1991; *Bates*, 1992). The emission occurs from the $\left(O_2\left(b^1\Sigma_g^+\right)\right)$ state, which has been postulated to be formed directly by the three-body recombination reaction of atomic oxygen [*Chapman*, 1931], or by this same recombination process producing an intermediate state which is subsequently collisionally quenched to the b^1 state [e.g., *Solheim and Llewellyn*, 1979; *Greer et al.*, 1981]. In the latter process, the intermediate state is believed to be $\left(O_2\left(c^1\Sigma_u^-\right)\right)$, which is also the precursor for the Herzberg II emission.

Any fundamental differences that might exist between these two proposed mechanisms for the excitation of the O_2 atmospheric emission, such as those associated with the

Paper number 92JA02348.
0148-0227/93/92JA-02348 $05.00

quenching of the b^1 and c^1 states, might reveal themselves in models and/or observations of wave-driven fluctuations in the emission. This is because various species will fluctuate out of phase with respect to each other under the influence of a wave [e.g., *Walterscheid et al.*, 1987], and also quenching is altitude dependent. Differences were not found in the modeling results of *Tarasick and Shepherd* [1992a, p. 3189], who concluded "Gravity wave observations will not be able to distinguish between a direct and an indirect process that both result in the same products, unless there is significant loss of the intermediate via other pathways." As we shall see, their results were insensitive to the production mechanism of the $O_2\left(b^1\Sigma_g^+\right)$ state primarily because they ignored the quenching effects of atomic oxygen. We will show that our calculated values of $\langle\eta\rangle$ are sensitive to the quenching effects of atomic oxygen and hence also to the production mechanism of the $O_2\left(b^1\Sigma_g^+\right)$ state.

Quenching of $O_2\left(c^1\Sigma_u^-\right)$ by atomic oxygen has been included in the model of *Zhang et al.* [1992b] using the empirical fitting parameter of *McDade et al.* [1986], but they did not include atomic oxygen quenching of $O_2\left(b^1\Sigma_g^+\right)$. Their calculated values of η did not exhibit a strong dependence on the reaction scheme employed, and they also concluded that measurements of η will not help to resolve any questions about the relative importance of the chemical excitation mechanisms.

In this paper we model the emission fluctuations of the O_2 atmospheric $\left(O_2\left(b^1\Sigma_g^+\right)\right)$ nightglow due to gravity waves, evanescent waves, and acoustic waves using the basic model formalism of *Schubert et al.* [1991] and employing the complex chemical scheme described in the theory section. Here, unlike *Tarasick and Shepherd* [1992a] and *Zhang et al.* [1992b], we incorporate the nonisothermal contributions to the intensity-weighted temperature in our calculations of $\langle\eta\rangle$, as described by *Schubert and Walterscheid* [1988], and we include the effects of diffusion of heat and momentum in the gravity wave dynamics, as described by *Hickey* [1988a] and *Schubert et al.* [1991]. We compare our calculated values of η with those derived from the observations of *Zhang* [1991] and *Zhang et al.* [1992a]. These observations, which were obtained during the AIDA (Arecibo Initiative in Dynamics of the Atmosphere) Act '89 campaign at Arecibo (18°N) during the period covering April 5 to May 9, 1989, were made with the MORTI (mesopause oxygen rotational temperature imager) instrument and provide us with values of $\langle\eta\rangle$ and the horizontal wavelengths and periods of the gravity waves. A complete discussion of the MORTI instrument, which is a spatial spectral scanning Fabry-Perot spectrometer, is given by *Wiens et al.* [1991]. There have been other measurements made of the O_2 Atmospheric (0-1) nightglow with subsequent determinations of $\langle\eta\rangle$ [e.g., *Viereck and Deehr*, 1989], but in those studies the horizontal wavelengths of the observed waves were unknown.

The layout of this paper is as follows. In the theory section we review the chemistry relevant to the O_2(0-1) nightglow emission and discuss the values of the pertinent parameters that we adopt here. The equations describing the fluctuations of the minor species are also derived. Next follows the results section, in which the first subsection the results are general in nature and investigate the effects of varying horizontal wavelength, wave period, chemical scheme, and season. In the second subsection the results are a direct comparison with the data of *Zhang* [1991]. A discussion and conclusions follow.

THEORY

The basic model formalism follows that of *Schubert et al.* [1991], except that we employ the chemistry appropriate to the O_2 atmospheric emission. Here, as in the work by *Hickey et al.* [1992], we employ a basic state derived from the model of *Garcia and Solomon* [1985]. We use their nighttime values of atomic oxygen number densities and their diurnally averaged values for the major gas density (N_2 and O_2), the temperature and the eddy diffusivities. The significance of using these model-derived values is that they are all calculated self-consistently, in contrast to some previous studies in which the eddy diffusivities were arbitrarily chosen and prescribed to be altitude independent. For consistency with *Garcia and Solomon* [1985], the Prandtl number is taken equal to 2 in the calculation of the thermal diffusivity.

The reactions appropriate for the O_2 atmospheric (0-1) band nightglow are listed in Table 1. We employ both the three-body recombination (Chapman) and the two-step (Barth) mechanisms for the production of the $O_2\left(b^1\Sigma_g^+\right)$ state. A good review of the nocturnal O_2 chemistry is given by *Torr et al.* [1985]. Unlike *Tarasick and Shepherd* [1992a], we include the loss of both $O_2\left(b^1\Sigma_g^+\right)$ and $O_2\left(c^1\Sigma_u^-\right)$ by quenching with atomic oxygen.

Some of the parameters listed in Table 1 deserve further

TABLE 1. Reaction Rates and Coefficients [after *Torr et al.*, 1985]

Reaction	Coefficient	Source
$O + O + M \rightarrow O_2 + M$	$k_1 = 4.7 \times 10^{-33} (300/T)^2$ cm^6 s^{-1}	*Campbell and Gray* [1973]
$O + O + M \rightarrow O_2(b^1\Sigma) + M$	$k = ek_1$, $e = 0.11$	*Deans et al.* [1976]: see text
$O + O + M \rightarrow O_2(c^1\Sigma) + M$	$k = \xi k_1$, $\xi = 0.8$	*Solheim and Llewellyn* [1979]
		Greer et al. [1981]: see text
$O_2(c^1\Sigma) + O_2 \rightarrow O_2(b^1\Sigma) + O_2$	$k_2 = 5 \times 10^{-13}$ cm^3 s^{-1}	*Greer et al.* [1981]
$O_2(c^1\Sigma) + O \rightarrow O_2 + O$	$(1 - \gamma)k_3$, $k_3 = 3 \times 10^{-11}$ cm^3 s^1	*Greer et al.* [1981]
$\rightarrow O_2(b^1\Sigma) + O$	γk_3, $\gamma = 0$, 0.1 or 0.2	*Torr et al.* [1985]: see text
$O_2(b^1\Sigma) + O \rightarrow O_2 + O$	$k_4 \leq 8 \times 10^{-14}$ cm^3 s^{-1}	*Slanger and Black* [1979]
$O_2(b^1\Sigma) + N_2 \rightarrow O_2 + N_2$	$k_5 = 2.2 \times 10^{-15}$ cm^3 s^{-1}	*Martin et al.* [1976]
$O_2(b^1\Sigma) + O_2 \rightarrow 2O_2$	$k_6 = 4.0 \times 10^{-17}$ cm^3 s^{-1}	*Martin et al.* [1976]
$O_2(c^1\Sigma) \rightarrow O_2 + h\nu$ (Herzberg II bands)	$A_1 = 10^{-3}$ to 2×10^{-2} s^{-1}	*Krupenie* [1972], *Slanger* [1978]
$O_2(b^1\Sigma) \rightarrow O_2 + h\nu$ (atmospheric bands)	$A_2 = 0.083$ s^{-1}	*Deans et al.* [1976]

comment. We employ a value of 0.11 for e because, as discussed by *Deans et al.* [1976], use of the equation for k_1 given by *Campbell and Gray* [1973] requires a decrease of the efficiency of excitation of 35% over the Deans et al. value of 0.17 (our calculations reveal that the required correction is closer to 41%). The production of $O_2\left(b^1\Sigma_g^+\right)$ by deactivation of the $O_2\left(c^1\Sigma_u^-\right)$ state by O has been conjectured by *Torr et al.* [1985] who investigated the effect of a branching ratio (γ) of 0.1 and 0.2. For most of our results we will assume that $\gamma = 0$, but we do study the sensitivity of our results to values of $\gamma =$ 0.1 and 0.2. The parameter ξ, the efficiency for production of $O_2\left(c^1\Sigma_u^-\right)$ in the association step, has been taken to be 0.8 [*Solheim and Llewellyn*, 1979; *Greer et al.* 1981], but the recent analysis of *Stegman and Murtagh* [1991] suggests that it is much smaller than this with an upper limit of about 0.1. We do not investigate the consequences of using values of ξ smaller than 0.8 because the derived results would then converge to those which include the formation of $O_2\left(b^1\Sigma_g^+\right)$ directly by the three-body recombination reaction alone.

First, we discuss the derivation of the perturbation equations applicable to the two-step process because the equations for the three-body recombination reaction are a simplification of these.

In the Eulerian reference frame, the continuity equation for the individual species perturbation number density is written [e.g., *Walterscheid et al.*, 1987]

$$i\omega n' = P' - L' - \bar{n} f(\bar{n}) \frac{T'}{T} \tag{1}$$

where

$$f(\bar{n}) = f_1 - f_2 / H(\bar{n}) .$$

Here, n is the species number density, T is temperature, and P and L are chemical production and loss terms, respectively; ω is the circular frequency of the wave perturbation; and $H(\bar{n})$ is the scale height of the undisturbed constituent. An overbar denotes an unperturbed state while a prime denotes a perturbed state. The dynamical factors f_1, f_2 and f_3 are described in detail by *Walterscheid et al.* [1987], *Hickey* [1988a] and *Schubert et al.* [1991]. The chemical production and loss terms can be derived from the set of reactions given in Table 1 and are provided in Table 2.

For O_2, N_2, and the major gas M (= O_2 + N_2), we can write

$$n'(\mathrm{M}) = f_3 \bar{n}(\mathrm{M}) \frac{T'}{T} \tag{2}$$

TABLE 2. Production and Loss Terms

State	P	L
O	–	$(1+e+\xi)k_1 n^2(\mathrm{O}) n(\mathrm{M})$
$O_2\left(c^1\Sigma_u^-\right)$	$ek_1 n^2(O) n(M)$	$k_2 n\left\{O_2\left(c^1\Sigma_u^-\right)\right\} n(O_2)$
		$+k_3 n\left\{O_2\left(c^1\Sigma_u^-\right)\right\} n(\mathrm{O})$
		$+A_1 n\left\{O_2\left(c^1\Sigma_u^-\right)\right\}$
$O_2\left(b^1\Sigma_g^+\right)$	$ek_1 n^2(\mathrm{O}) n(M)$	$k_4 n\left\{O_2\left(b^1\Sigma_g^+\right)\right\} n(\mathrm{O})$
	$+k_2 n(O_2) n\left\{O_2\left(c^1\Sigma_u^-\right)\right\}$	$+k_5 n\left\{O_2\left(b^1\Sigma_g^+\right)\right\} n(N_2)$
	$+\gamma k_3 n(\mathrm{O}) n\left\{O_2\left(c^1\Sigma_u^-\right)\right\}$	$+k_6 n\left\{O_2\left(b^1\Sigma_g^+\right)\right\} n(O_2)$
		$+A_2 n\left\{O_2\left(b^1\Sigma_g^+\right)\right\}$

while for O,

$$i\omega n'(\mathrm{O}) = -L'(\mathrm{O}) - \bar{n}(\mathrm{O}) f(\bar{n}(\mathrm{O})) \frac{T'}{T} \tag{3}$$

where

$$L'(\mathrm{O}) = (1+e+\xi)\left\{k_1 n^2(\mathrm{O}) n(\mathrm{M})\right\}' . \tag{4}$$

Upon expansion of (4) for L'(O) and neglect of nonlinear terms, (3) becomes

$$\begin{aligned} &\left\{i\omega + 2\bar{k}_1(1+e+\xi)\bar{n}(\mathrm{O})\bar{n}(\mathrm{M})\right\} n'(\mathrm{O}) \\ &= \left\{(2-f_3)(1+e+\xi)\bar{k}_1 \bar{n}^2(\mathrm{O})\bar{n}(\mathrm{M}) - \bar{n}(\mathrm{O}) f(\bar{n}(\mathrm{O}))\right\} \frac{T'}{T} \end{aligned} \tag{5}$$

For $O_2\left(c^1\Sigma_u^-\right)$ we get

$$\begin{aligned} &\left\{i\omega + k_2\bar{n}(O_2) + k_3\bar{n}(\mathrm{O}) + A_1\right\} n'\left(O_2\left(c'\Sigma\right)\right) \\ &= \left\{(f_3-2)\xi\bar{k}_1\bar{n}^2(\mathrm{O})\bar{n}(\mathrm{M}) \right. \\ &\quad \left. - \left[f_3 k_2 \bar{n}(O_2) + f\left(\bar{n}\left(O_2\left(c^1\Sigma\right)\right)\right)\right]\bar{n}\left(O_2\left(c^1\Sigma\right)\right)\right\}\frac{T'}{T} \\ &\quad + \left[2\xi\bar{k}_1\bar{n}(\mathrm{O})\bar{n}(\mathrm{M}) - k_3\bar{n}\left(O_2\left(c^1\Sigma\right)\right)\right] n'(\mathrm{O}) \end{aligned} \tag{6}$$

while for $O_2\left(b^1\Sigma_g^+\right)$ we arrive at

$$\begin{aligned} &\left\{i\omega + k_4\bar{n}(\mathrm{O}) + k_5\bar{n}(N_2) + k_6\bar{n}(O_2) + A_2\right\} \\ &\times n'\left(O_2\left(b^1\Sigma\right)\right) = \left\{(f_3-2)e\bar{k}_1\bar{n}^2(\mathrm{O})\bar{n}(\mathrm{M}) \right. \\ &\quad + k_2 f_3 \bar{n}(O_2)\bar{n}\left(O_2\left(c^1\Sigma\right)\right) - \bar{n}\left(O_2\left(b^1\Sigma\right)\right) \\ &\quad \times \left. \left[f_3 k_5 \bar{n}(N_2) + f_3 k_6 \bar{n}(O_2) + f\left(\bar{n}\left(O_2\left(b^1\Sigma\right)\right)\right)\right]\right\}\frac{T'}{T} \\ &\quad + \left[2e\bar{k}_1\bar{n}(\mathrm{O})\bar{n}(\mathrm{M}) + \gamma k_3\bar{n}\left(O_2\left(c^1\Sigma\right)\right) - k_4\bar{n}\left(O_2\left(b'\Sigma\right)\right)\right] \\ &\quad \times n'(\mathrm{O}) + \left[k_2\bar{n}(O_2) + \gamma k_3\bar{n}(\mathrm{O})\right] n'\left(O_2\left(c^1\Sigma\right)\right) \end{aligned} \tag{7}$$

The equivalent set of reactions appropriate for the three-body recombination process alone are found by setting to zero all those constants associated with the $O_2\left(c^1\Sigma_u^-\right)$ state (i.e., ξ, k_2, k_3, A_1), so that

$$\begin{aligned} &\left\{i\omega + 2\bar{k}_1(1+e)\bar{n}(\mathrm{O})\bar{n}(\mathrm{M})\right\} n'(\mathrm{O}) \\ &= \left\{(2-f_3)(1+e)\bar{k}_1\bar{n}(\mathrm{O})\bar{n}(\mathrm{M}) - \bar{n}(\mathrm{O}) f(\bar{n}(\mathrm{O}))\right\}\frac{T'}{T} \end{aligned} \tag{8}$$

and

$$\begin{aligned} &\left\{i\omega + k_4\bar{n}(\mathrm{O}) + k_5\bar{n}(N_2) + k_6\bar{n}(O_2) + A_2\right\} n'\left(O_2\left(b^1\Sigma\right)\right) \\ &= \left\{(f_3-2)e\bar{k}_1\bar{n}^2(\mathrm{O})\bar{n}(\mathrm{M}) - \bar{n}\left(O_2\left(b^1\Sigma\right)\right)\right. \\ &\quad \times \left. \left[f_3 k_5 \bar{n}(N_2) + f_3 k_6 \bar{n}(O_2) + f\left(\bar{n}\left(O_2\left(b^1\Sigma\right)\right)\right)\right]\right\}\frac{T'}{T} \\ &\quad + \left[2e\bar{k}_1\bar{n}(\mathrm{O})\bar{n}(\mathrm{M}) - k_4\bar{n}\left(O_2\left(b^1\Sigma\right)\right)\right] n'(\mathrm{O}) . \end{aligned} \tag{9}$$

The equations for the unperturbed species $O_2\left(b^1\Sigma_g^+\right)$ and $O_2\left(c^1\Sigma_u^-\right)$ number densities and scale heights are given in the appendix. Given $\bar{n}\left(O_2\left(b^1\Sigma_g^+\right)\right)$ and $n'\left(O_2\left(b^1\Sigma_g^+\right)\right)$, the fractional fluctuation in the O_2 (0-1) band nightglow intensity due to gravity waves is simply $I'/\bar{I} = n'/\bar{n}$. We can proceed to calculate Krassovsky's ratio $\langle\eta\rangle$ for an extended emission layer following *Schubert and Walterscheid* [1988], where $\langle\eta\rangle = (\langle I'\rangle/\langle\bar{I}\rangle)/(\langle T_I'\rangle/\langle\bar{T}_I\rangle)$ the brackets denote an altitude integration, I is intensity, and the temperatures are intensity-weighted (hence the subscript I).

Results

For all of our results the undisturbed mesosphere is defined by the model output of Garcia and Solomon [1985] for a latitude of 18°N and for the months of March and June, these being most relevant to the observations made at Arecibo by *Zhang* [1991] and *Zhang et al.* [1992a]. Figures 1a to 1c show the undisturbed temperatures, eddy diffusivities and atomic oxygen densities, respectively, versus altitude. These profiles have been discussed by *Hickey et al.* [1992] and will not be discussed further here.

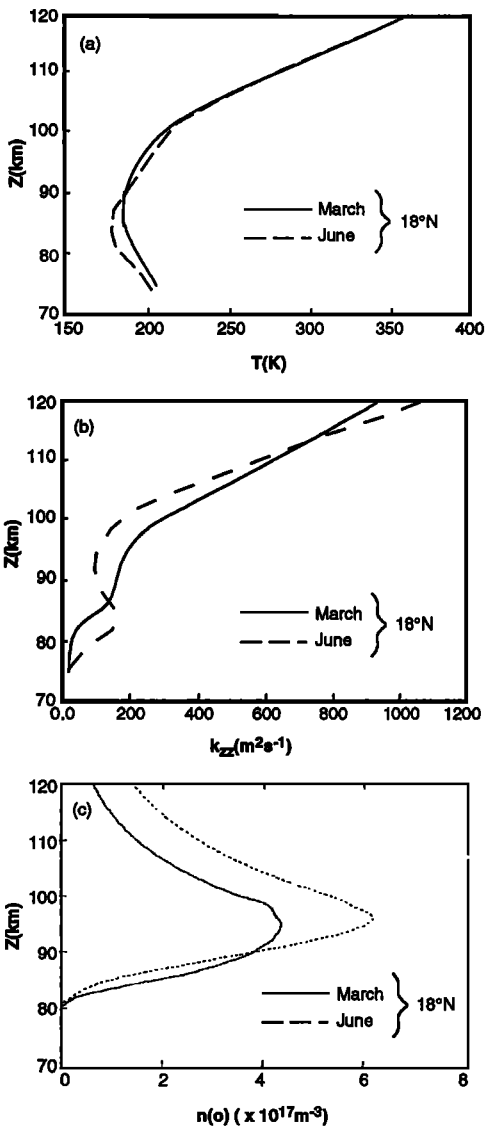

Fig. 1. (a) Undisturbed temperatures, (b) eddy diffusivities, and (c) atomic oxygen number densities at 18°N for March (solid) and June (dotted).

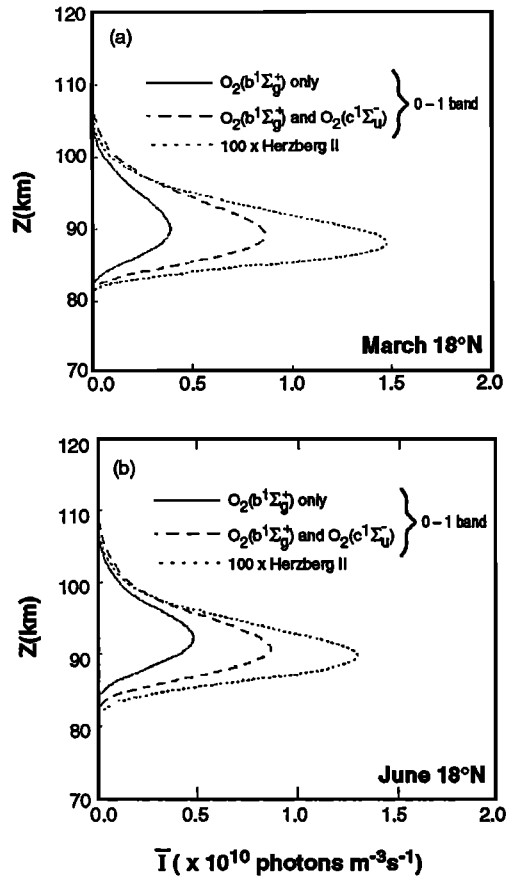

Fig. 2. Undisturbed nightglow intensities of the O_2 atmospheric (0-1) band (solid and dotted) and the Herzberg II band (dashed) at 18°N for (a) March and (b) June. See text for details.

The undisturbed nightglow intensity profiles derived from these parameters are plotted in Figures 2a and 2b for March and June, respectively. In each of these figures we show the O_2 (0-1) band intensities calculated using the three-body recombination reaction scheme alone or with the further inclusion of the two-step reaction scheme. In the case of the two-step reaction scheme we also show the calculated profile of the Herzberg II band intensities that derive from the $c^1\Sigma_u^- - X^3\Sigma_g^-$ transition.

General Results

In the first set of results we employ the nominal reaction coefficients listed in Table 1 and the mean state described above to calculate the O_2 (0-1) band nightglow fluctuations as a function of wave period and horizontal disturbance wavelength λ_x. Because $\langle\eta\rangle$ is determined in part by wave dynamics, we first discuss the real and imaginary parts of the complex wavenumber k_z. The equations for the internal gravity waves that we use have been thoroughly derived and explained before [e.g., *Walterscheid et al.*, 1987; *Hickey and Cole*, 1987; *Hickey*, 1988a; *Schubert et al.*, 1991] and will not be repeated here.

The vertical wavelength ($\lambda_z = 2\pi\{\mathrm{Re}(k_z)\}^{-1}$) and the imaginary part of the vertical wavenumber ($\mathrm{Im}(k_z)$) are shown as a function of wave period in Figures 3 (λ_x = 100 km), 4 (λ_x = 500 km), and 5 (λ_x = 1000 km). In Figures 3a, 4a, and 5a we display λ_z while $\mathrm{Im}(k_z)$ is shown in Figures 3b, 4b, and 5b.

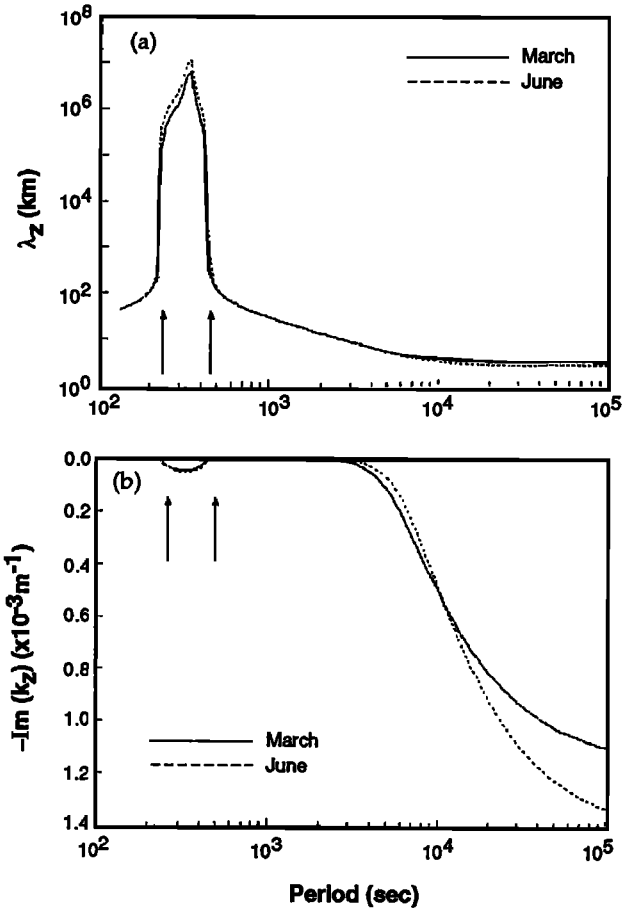

Fig. 3. (a) Vertical wavelength and (b) the imaginary part of k_z for March (solid) and June (dotted) at 18°N as a function of wave period for a horizontal wavelength (λ_x) of 100 km. The arrows define the approximate extent of the evanescent region.

Although the standard $1/2H$ term is not included in the values of the imaginary part of k_z shown in these figures, it has nonetheless been included in all of our computations. There are two curves in each figure for the months of March and June. The periods in these figures extend from 100 s to 10^5 s, covering the period range from long-period acoustic waves, through evanescent waves to long-period gravity waves. The approximate periods marking the extent of the evanescent region appropriate for conditions near the peak of the undisturbed emission (93 km altitude) are indicated with arrows on the figures. These periods were calculated using the basic dispersion equation of Hines [1960].

In Figures 3a, 4a, and 5a we can see that at evanescent periods λ_z is slightly greater in June than it is in March and is many orders of magnitude greater than it is for the internal waves. Without dissipation, λ_z is infinite for evanescent waves. In our evanescent wave results λ_z is real and it assumes values between about 10^3 km and 10^7 km, which is large by atmospheric standards (the scale height is about 5.5 km). Although the dissipation is extremely small for the evanescent waves, its inclusion forces Re(k_z) to be nonzero (albeit large). The values of λ_z at internal periods are symmetric about the evanescent region, although we do not consider short-period acoustic waves. As we increase period at internal gravity wave periods, λ_z decreases and at long periods asymptotes to a constant. At these longest periods, λ_z is greater in March than it is in June. As the horizontal wavelength is increased, the vertical wavelength at almost all periods increases while the evanescent region broadens (in the period domain) and shifts toward larger periods.

In Figures 3b, 4b, and 5b we can see that Im(k_z) is approximately zero at the long acoustic periods and the short gravity wave periods. As we progress to longer gravity wave periods, Im(k_z) becomes more negative as the dissipation increases. Also, the period at which |Im(k_z)| begins to increase occurs at progressively larger values as λ_x increases. At evanescent periods |Im(k_z)| is negative and becomes more negative toward the center of the evanescent region. The maximum value of |Im(k_z)| in the evanescent region increases slightly with increasing λ_x. For evanescent waves, Im(k_z) is given by

$$\mathrm{Im}(k_z) = 1/2H - \left\{k_x^2\left(1-\omega_g^2/\omega^2\right)+\left(\omega_a^2-\omega^2\right)/C^2\right\}^{1/2} \qquad (10)$$

where all terms have their usual meanings [e.g., *Hines*, 1960]. This solution, which has a negative sign preceding the term within braces, is chosen over the solution having a corresponding positive sign, to ensure that the total wave energy density in an infinite column of air remains finite. Our numerical results for Im(k_z) for the evanescent waves, which have been plotted in Figures 3b to 5b (and where, in keeping with our results for the internal waves in which we display the contributions to Im(k_z) due solely to dissipation, we have chosen not to display the $1/2H$ contribution), are equivalent to the numerical value of the term enclosed within braces of the above equation.

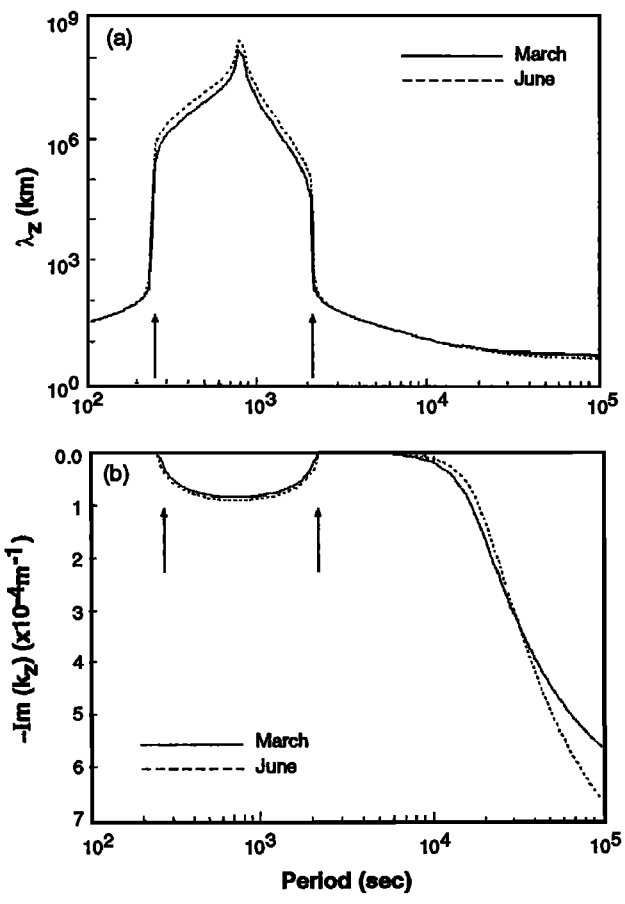

Fig. 4. Same as Figure 3 except that λ_x = 500 km.

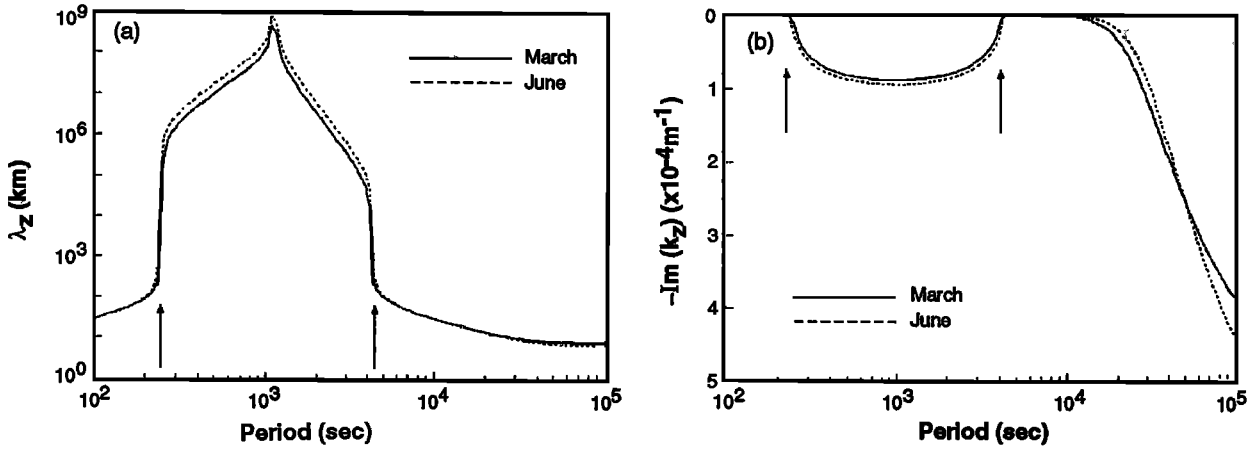

Fig. 5. Same as Figure 3 except that λ_x = 1000 km.

Values of <η> are shown in Figures 6 (λ_x = 100 km), 7 (λ_x = 500 km) and 8 (λ_x = 1000 km). The amplitude of <η> is shown in Figures 6a, 7a, and 8a while its phase is shown in Figures 6b, 7b, and 8b. There are four curves in each figure, corresponding to the months of March and June, the three-body reaction scheme alone, and the further inclusion of the two-step reaction scheme.

In Figure 6a there is a general increase in |<η>| with increasing wave period (with some interference-related oscillations at intermediate periods) and an asymptotic approach to a constant at long periods. The interference-related oscillations are larger when the three-body reaction scheme operates alone. This is especially noticeable for periods between about 1 and 2 hours. For periods greater than about 0.5 hour, March values of |<η>| exceed those of June while for smaller periods the reverse is true. Large discontinuities occur in |<η>| at the short-period end of the evanescent region; these are noticeably larger with the inclusion of the two-step reaction scheme in March.

The phase of <η> at acoustic periods is seen in Figure 6b to

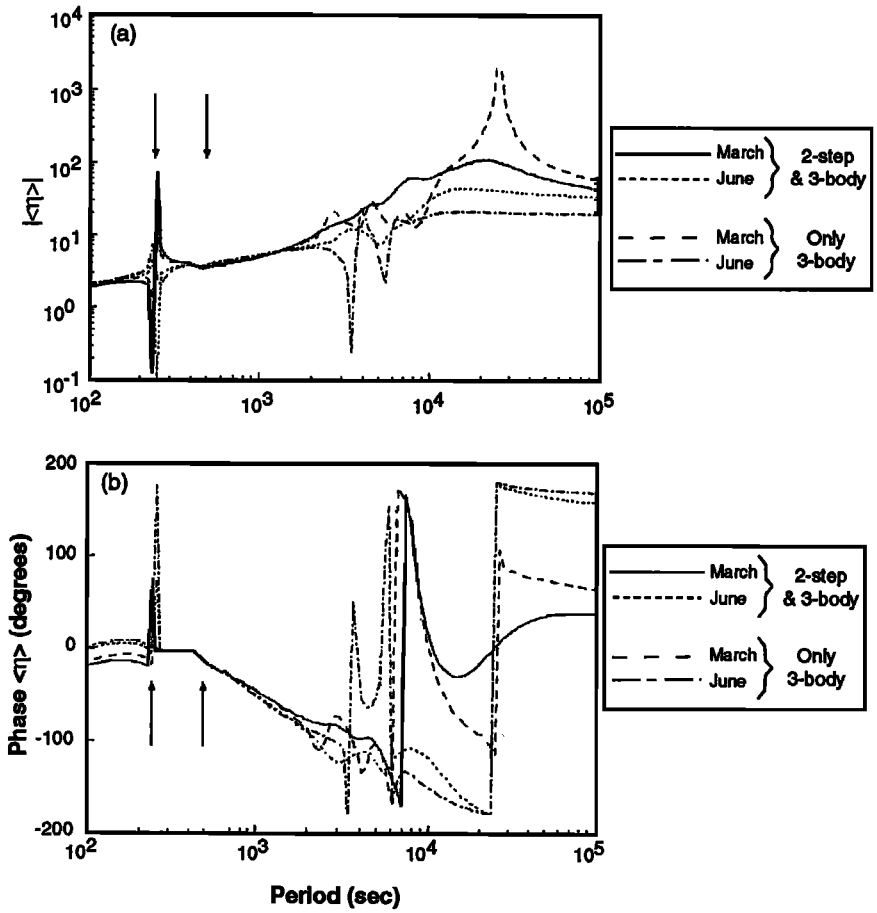

Fig. 6. (a) Magnitude and (b) phase of the parameter <η> at 18°N and for λ_x = 100 km. See text for details. The arrows define the approximate extent of the evanescent region.

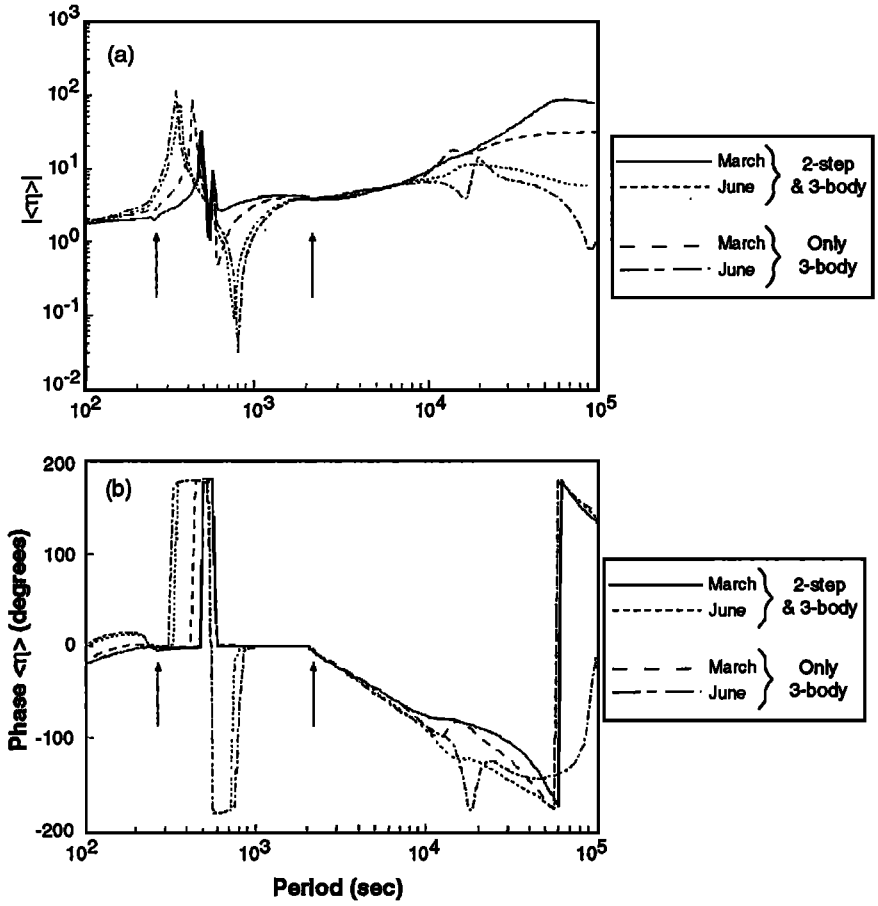

Fig. 7. Same as Figure 6 except that $\lambda_x = 500$ km.

depend more on the undisturbed atmosphere than on the reaction scheme. At short evanescent periods the phase of <η> increases and then decreases very abruptly, after which it remains approximately constant. As the period increases into the gravity wave regime, the phase of <η> decreases steadily subject to some modification due to the effects of interference at periods of 0.5 hour or more. At very long periods (>8 hours) the phase of <η> is again more sensitive to the state of the undisturbed atmosphere than it is to the particular reaction scheme. The large swings in the phase of <η> at periods of hours are associated more with the definition that it be between ±180° than with interference effects.

In Figure 7a ($\lambda_x = 500$ km) there is a general increase in |<η>| with increasing wave period that is interrupted by sharp variations in |<η>| in the evanescent wave regime. At longer gravity wave periods the effects of interference are more noticeable for results obtained with the three-body recombination scheme than with those obtained with the further inclusion of the two-step scheme. At the longest periods, |<η>| is considerably larger in March than in June and, for a given month, it is also considerably larger for the reaction scheme that includes the two-step reaction.

For $\lambda_x = 500$ km, the phase of <η> at acoustic periods (Figure 7b) is similar to that shown in Figure 6b ($\lambda_x = 100$ km) at similar periods, indicating that the phase of <η> is insensitive to λ_x at acoustic periods. The evanescent region is very broad, ranging from periods of about 4 min to 35 min or more. The phase of <η> (Figure 7b) associated with periods less than the midpoint of the period range of the evanescent region initially increases rapidly to 180° and then remains approximately constant (it actually increases slightly beyond 180°, accounting for the abrupt change in phase to about -180°). At periods slightly greater than the midpoint of the evanescent region the phase rapidly changes to zero, and then remains so until internal gravity wave periods are reached. The extent in period of the region of constant phase at evanescent periods depends strongly on season and the reaction scheme employed (Figure 7b). It is broader in March and also when the two-step reactions are included. At gravity wave periods the phase decreases uniformly except for some interference-related peaks at periods of about 5 hours. These only occur for the results which include the three-body recombination scheme alone.

The results for $\lambda_x = 1000$ km shown in Figure 8 resemble those shown in Figure 7 for $\lambda_x = 500$ km. The main differences are that for the larger value of λ_x the evanescent region extends to greater periods, while at long periods both the magnitude and phase of <η> are less sensitive to season or to the inclusion of the two-step reaction scheme.

In summary, these results have shown that at evanescent and short gravity wave periods it is not possible to discriminate between seasonal effects and between the effects of different chemical schemes. However, at very long gravity wave periods and also at the shortest acoustic wave periods that we studied, such a discrimination appears to be possible.

In Figures 9a and 9b we show the sensitivity of our calculated values of <η> to the values of the quenching parameters k_3 and k_4, and the branching ratio γ. We have performed calculations for the March 18°N set of atmospheric parameters, and for $\lambda_x =$

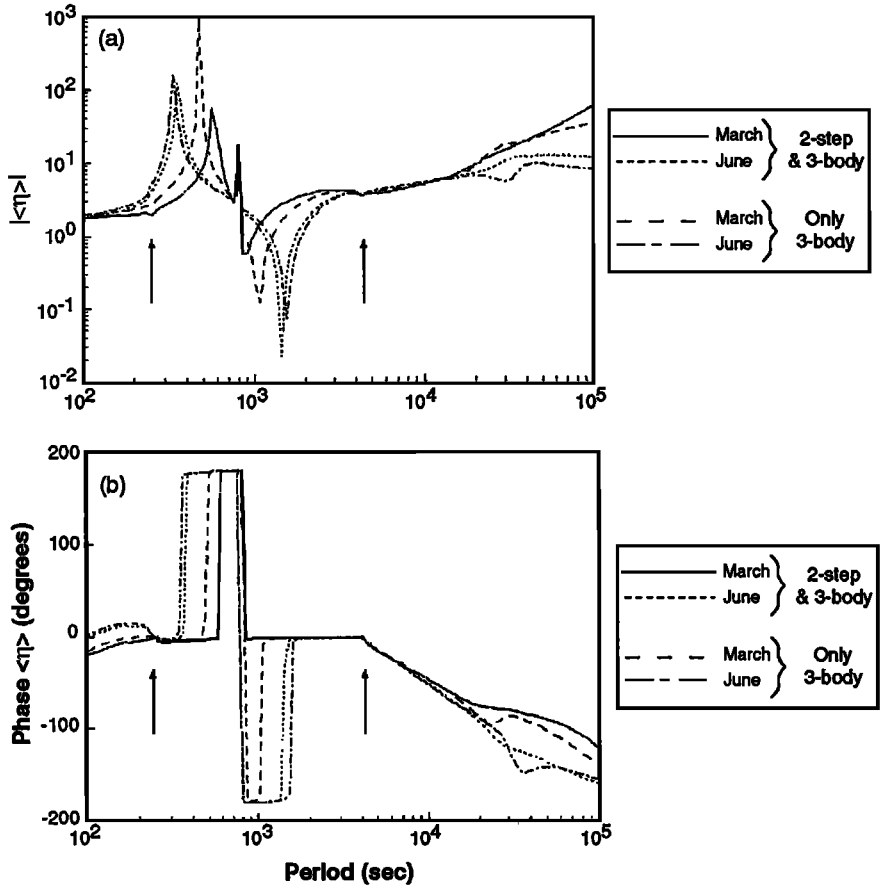

Fig. 8. Same as Figure 7 except that $\lambda_x = 1000$ km.

100 km. The solid curve in each panel corresponds to the three-body reaction scheme alone calculated using the nominal reaction kinetic parameters, while the other three curves correspond to production of $O_2\left(b^1\Sigma_g^+\right)$ by both the three-body and the two-step reaction schemes. The first of these three curves corresponds to calculations using the nominal reaction kinetic parameters, the second curve corresponds to these nominal parameters with the exception that both k_3 and k_4 have been set to zero, and the third curve corresponds to the nominal parameters with the exception that γ has been set to 0.2.

We can see that both the amplitude (Figure 9a) and the phase (Figure 9b) of <η> are the least sensitive to the reaction kinetic parameters at acoustic and short gravity wave periods, with strong sensitivity at evanescent periods. At longer gravity wave periods the values of <η> calculated for $\gamma = 0.2$ lie between those two sets of <η> values that were calculated using the nominal reaction kinetic parameters for the three-body

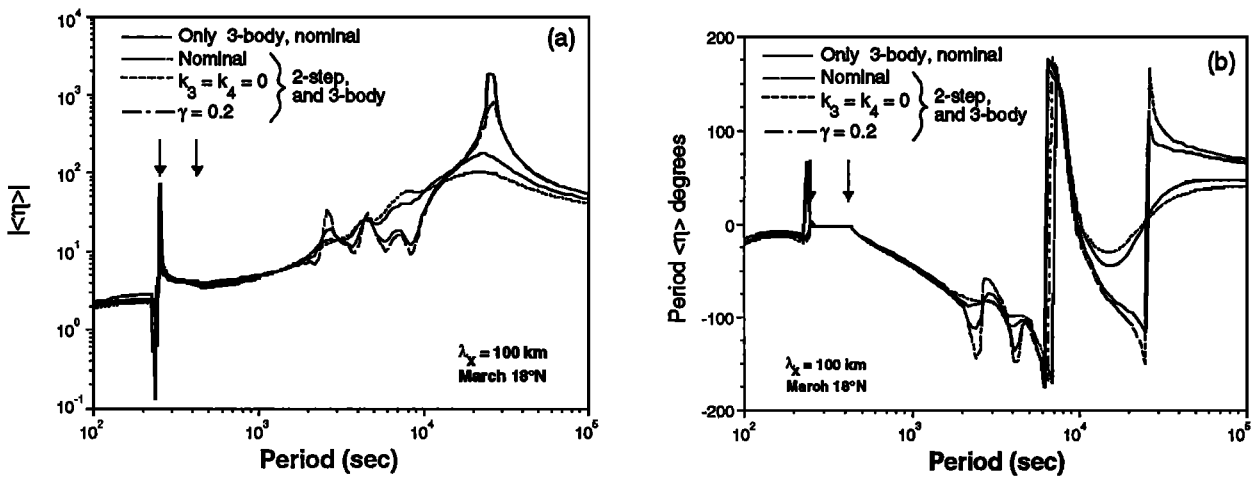

Fig. 9. (a) Magnitude and (b) phase of the parameter <η> for March at 18°N and for a horizontal wavelength (λ_x) of 100 km. Calculations are for the three-body reaction scheme alone and nominal reaction kinetic parameters (solid) while the other three curves are for the complete chemistry and for nominal reaction kinetic parameters (dotted), $k_3 = k_4 = 0$ (dashed) and $\gamma = 0.2$ (dashed-dotted). The arrows define the approximate extent of the evanescent region.

recombination reaction alone and for both the three-body and two-step reaction schemes included together. This is as we expected, because the nonzero value of γ diminishes the concentration of $O_2\left(c^1\Sigma_u^-\right)$ and increases the concentration of $O_2\left(b^1\Sigma_g^+\right)$, thereby increasing the importance of the three-body recombination reaction.

When quenching by atomic oxygen is ignored (i.e., k_3 and k_4 are set to zero), the resulting values of $<\eta>$ are similar to those obtained from the three-body recombination scheme alone. This explains why *Tarasick and Shepherd* [1992a], who ignored the effects of quenching by atomic oxygen, were unable to discriminate between the two production mechanisms for the $O_2\left(b^1\Sigma_g^+\right)$.

We have also tested the sensitivity of our modeled values of $<\eta>$ to the radiative lifetime of the $O_2\left(c^1\Sigma_u^-\right)$ state by decreasing A_1 from its nominal value of 2.2 x $10^{-2}s^{-1}$ to $10^{-3}s^{-1}$. This change has a negligibly small effect on $<\eta>$ at acoustic and gravity wave periods, but decreases the magnitude of the discontinuity in $|<\eta>|$ and increases the magnitude of the discontinuity in the phase of $<\eta>$ at evanescent periods.

Comparison With Data

In this subsection we compare our model derived values of $<\eta>$ with those derived from observations of the O_2 atmospheric nightglow [*Zhang*, 1991; *Zhang et al.*, 1992b]. We calculate $<\eta>$ for the values of λ_x and wave period provided by *Zhang* [1991] and *Zhang et al.* [1992a]. In some cases Zhang was able to determine intrinsic wave periods, in which cases only the intrinsic periods are displayed in our figures. The observations of *Zhang* [1991] and *Zhang et al.* [1992a] are summarized in Table 3. The wave type (internal gravity wave or evanescent wave) was defined using the dispersion equations of *Hines* [1960].

The results of our comparison of observed and calculated values of $<\eta>$ are shown in Figures 10 through 12. We limit our comparisons to ranges of periods that cover the observations. The results for the three evanescent waves are shown in Figure 10, while those for the 10 internal waves are shown in Figures 11 and 12.

TABLE 3. Summary of Zhang's [1991] Observations

Period min	λ_x km	Wave Type	$\|<\eta>\|$	Phase $<\eta>$
56*±5	228±30	internal	4.5±1.0	-2°±18°
82±5	456±45	internal	5.2±1.5	0°±9°
100*±10	505±60	internal	5.0±1.0	0°±6°
148*±5	774±70	internal	3.5±0.4	-1°±8°
162±5	890±80	internal	4.8±1.0	0°±5°
340±10	989±60	internal	5.5±1.5	0°±3°
75*±5	1040±90	evanescent	4.5±1.5	0°±10°
138±5	1296±120	internal	4.6±1.5	0°±6°
150±5	1497±140	internal	4.8±1.0	0°±5°
106±5	1795±60	evanescent	4.0±1.0	0°±7°
157*±10	2654±300	evanescent	3.7±0.5	-16°±17°
250*±10	2705±500	internal	5.5±1.0	-7°±11°
302*±10	2896±500	internal	3.5±1.0	0°±3°

* Intrinsic wave period.

The values of $|<\eta>|$ for the evanescent waves are shown in Figure 10a. For λ_x = 1040 km, the observed value of $|<\eta>|$ exceeds the modeled values. The observed values of $|<\eta>|$ lie within the bounds of the modeled values for the cases λ_x = 1795 and 2654 km. In the first of these cases (λ_x = 1795 km), the observed value of $|<\eta>|$ lies between the modeled values of $|<\eta>|$ that were calculated for March and June, with only a small dependence on the chemical scheme employed. In the second case (λ_x = 2654 km), the observed value of $|<\eta>|$ lies between the two modeled values of $|<\eta>|$ that were both calculated for June, with one using the three-body recombination scheme alone and the other using the complete chemistry. In all three cases, the modeled values of $|<\eta>|$ lay within the errors of the observed values of $|<\eta>|$. The phases of $<\eta>$ for the evanescent waves are shown in Figure 10b. Our modeled values of the phases are always close to 0°, in agreement with the observed

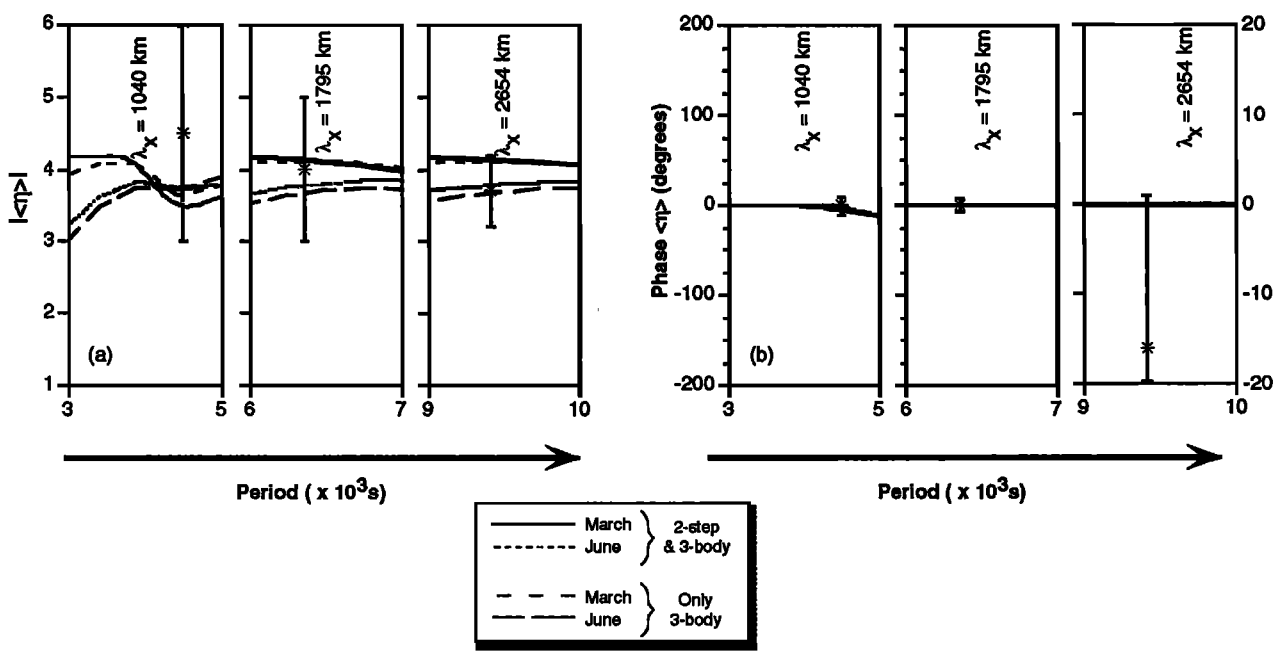

Fig. 10. (a) Magnitude and (b) phase of the parameter $<\eta>$ at 18°N for the evanescent waves listed in Table 3. Also shown are *Zhang's* [1991] measured values (*).

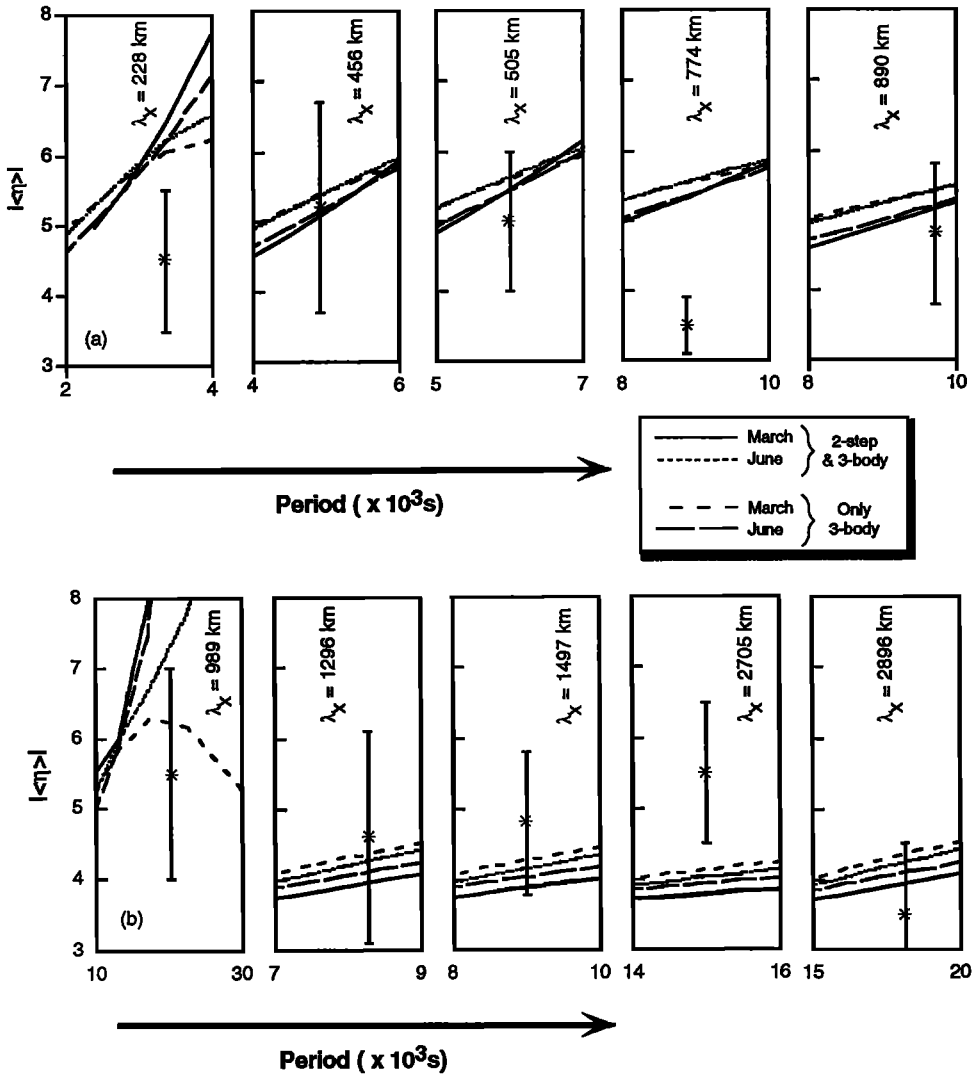

Fig. 11. Magnitude of the parameter <η> at 18°N for the internal waves listed in Table 3. Also shown are *Zhang's* [1991] measured values (*).

phases for λ_x = 1040 and 1795 km. However, the observed phase of <η> for λ_x = 2654 km is 16°. Our modeled phases of <η> do depend slightly on the chemical scheme and on season, but not in any consistent way.

The values of |<η>| for λ_x = 228, 456, 505, 774 and 890 km are shown in Figure 11a while those for λ_x = 989, 1296, 1497, 2705 and 2896 km are shown in Figure 11b. The observed values of |<η>| lie within the bounds of our modeled values only for the cases λ_x = 456 and 1296 km. In these two cases our modeled values of |<η>| display no obvious dependence on season or chemical scheme (these two waves were actually observed in early May). For the other wavelengths considered, the modeled values of |<η>| were sometimes smaller (6 cases) and sometimes greater (2 cases) than the observed values. Again, these differences show no consistent dependence on season or chemical scheme. Our modeled values of |<η>| never differed by more than 2 from the observed values, and in most cases the differences were closer to 0.5. The modeled values of |<η>| lay within the errors of the observed values of |<η>| for 6 of the 10 cases considered. The comparatively large errors in the observed values of |<η>| make it impossible to decide which chemical scheme used in the model provides the best results.

The phases of <η> for λ_x = 228, 456, 505, 774 and 890 km are shown in Figure 12a while those for λ_x = 989, 1296, 1497, 2705 and 2896 km are shown in Figure 12b. In every case the modeled phase differed considerably from the observed phase (which was usually 0°). However, the agreement between observed and modeled phases was significantly better for the four internal waves with the largest horizontal wavelengths. Again, for all of these phase comparisons, there appear to be no dependences on season or chemical scheme. The errors associated with the observed phases of <η> are minimal, and cannot account for the differences between the observed and modeled phases of <η>.

Discussion

Although our model includes the effects of diffusion of heat and momentum in the gravity wave dynamics, most of the waves that were observed by *Zhang* [1991] and *Zhang et al.* [1992a] and are listed in Table 3 were not affected by these dissipative effects. For one wave (λ_x = 989 km) the calculated value of <η> was affected by dissipation. However, while the inclusion of dissipation marginally improved the agreement between the modeled and observed phases of <η>, its inclusion worsened this agreement for the magnitude of <η>.

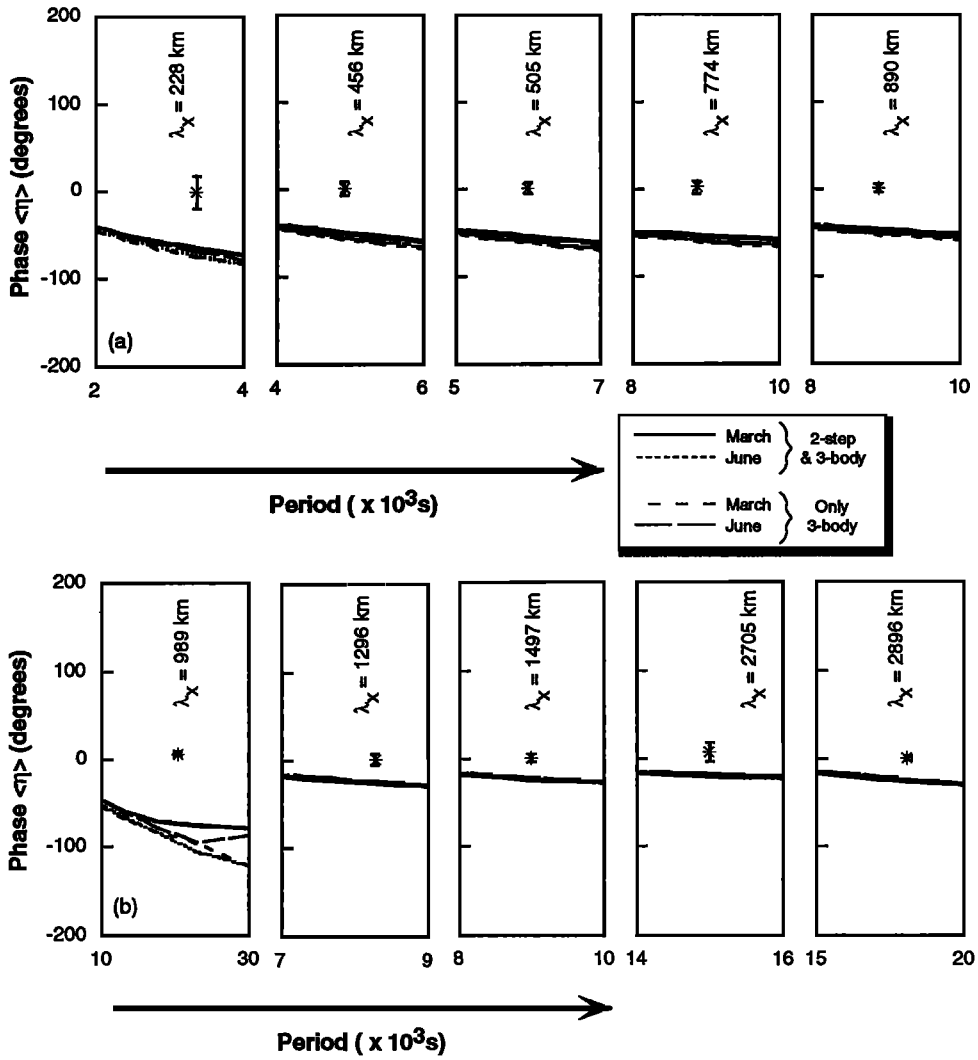

Fig. 12. Same as Figure 10 except for the phase of <η>.

Zhang et al. [1992b] compared their model with the observations of *Zhang* [1991] and *Zhang et al.* [1992a], and found similar overall agreement as we have found in our comparisons. In spite of the fact that dissipation appears to be unimportant for most of the observed waves, differences exist between our calculated values of <η> and those of *Zhang et al.* [1992b]. This is because there are other differences between these two models. First, we incorporate the nonisothermal contributions to the intensity-weighted temperature in our calculations of <η>, as described by *Schubert and Walterscheid* [1988], whereas they do not. Second, we include the quenching of $O_2\left(b^1\Sigma_g^+\right)$ by atomic oxygen. Last of all, our calculations are performed for a different set of atmospheric parameters than those of *Zhang et al.* [1992b]. We have repeated some of our calculations using the intensity-weighted temperature equation relevant to an isothermal atmosphere, and found that while this reduces the phase of <η> (thereby improving the agreement with the observations), it changes the magnitude of <η> in a random way that does not necessarily improve the agreement with the observations. The other differences between the two models cannot be readily assessed.

The chemical schemes we employed to determine <η> are still uncertain. Inspection of Table 1 shows that had we increased the value of e over its nominal value of 0.11 or decreased the value of ξ below its nominal value of 0.8 we would have increased the ratio $n\{O_2(b^1\Sigma)\}/n\{O_2(c^1\Sigma)\}$. Thus, for a given season the resulting values of <η> would lie somewhere between the results for the three-body recombination scheme alone and complete chemistry. *Stegman and Murtagh* [1991] have concluded from their measurements of the near-ultraviolet portion of the nightglow spectrum that all of the O_2 UV emissions are produced by a single-step recombination process. Their results place an upper limit on the production efficiency for $O_2\left(c^1\Sigma_u^-\right)$ that is only one-eighth of the nominal value given in Table 1. However, in his review of oxygen nightglow emissions, *Bates* [1992] has stated that termolecular association of oxygen atoms does not make an appreciable direct contribution to the atmospheric system, because the $O_2\left(b^1\Sigma_g^+\right)$ thus produced is mainly in high vibrational levels that do not experience rapid vibrational deactivation. We have repeated our calculations with the value of e in Table 1 reduced by a factor of 100, essentially removing the process of production of the $O_2\left(b^1\Sigma_g^+\right)$ state by the termolecular association of atomic oxygen atoms. The differences this makes in the values of <η> are minimal at short periods. At long periods <η> is reduced by up to 25% from its nominal value, increasing the differences between the values of <η> calculated with complete chemistry

and the three-body recombination scheme alone. The phase of $<\eta>$ is less sensitive to this change at long periods, and never differs by more than about 10° from its nominal value. Thus, the assertion of *Bates* [1992], if correct, would not significantly affect our results.

The differences between observed and modeled values of $<\eta>$ may be attributed to several contributing factors. We know that there are uncertainties associated with the chemistry, but our sensitivity tests reveal that this cannot be the sole contributor. We also know that climatological models cannot reproduce the variability that is observed from one night to the next in the mean atmospheric parameters. The average nighttime temperatures given by *Zhang* [1991] (these were not reported by *Zhang et al.* [1992a]) vary considerably from one night to the next. We would presume that the average distributions of the minor species, such as atomic oxygen, would also vary considerably from one night to the next. These effects are difficult to assess.

Lastly, it is quite possible that some of the observed emission fluctuations were due to saturating waves or due to waves that resembled wave packets rather than steady state, monochromatic waves. Thus, some of the disagreement between our modeled results and the observations may be attributable to unmodeled (although well understood) physics.

CONCLUSIONS

We have modeled the wave-driven fluctuations in the O_2 (0-1) atmospheric nightglow and calculated the parameter $<\eta>$ with a model that accounts for either three-body recombination of atomic oxygen atoms alone to form the $O_2\left(b^1\Sigma_g^+\right)$ state directly, or by the further inclusion of the process that allows formation of the $O_2\left(c^1\Sigma_u^-\right)$ intermediate state. We have performed our calculations for a latitude of 18°N and for the months of March and June, these being most relevant to the observations made at Arecibo by *Zhang* [1991] and *Zhang et al.* [1992a].

Our general results, which display how $<\eta>$ varies with wave period, horizontal wavelength, season and chemical scheme, have shown that for given values of wave period and horizontal wavelength it is not possible to discriminate between seasonal effects and between the effects of different chemical schemes at evanescent and short gravity wave periods. At the shortest acoustic wave periods that we studied, and also at very long gravity wave periods, such a discrimination appears possible.

We have shown that when quenching by atomic oxygen is ignored the resulting values of $<\eta>$ calculated with the complete chemistry are similar to those obtained from the three-body recombination scheme alone. This explains why *Tarasick and Shepherd* [1992a] were unable to discriminate between the two proposed production mechanisms for the $O_2\left(b^1\Sigma_g^+\right)$. In contrast, we have demonstrated that our calculated values of $<\eta>$ are sensitive to the quenching effects of atomic oxygen and hence also to the production mechanism of the $O_2\left(b^1\Sigma_g^+\right)$ state.

We compared our model-derived values of $<\eta>$ with those derived from observations of the O_2 atmospheric nightglow [*Zhang*, 1991] and found that for the evanescent waves (three cases) the observed values of $<\eta>$ essentially compared very well with the modeled values of $|<\eta>|$. Also, the modeled phases of $<\eta>$ are close to 0°, in agreement with the observed phases of $<\eta>$ for only 2 of the observations. For the 10 internal waves considered, the differences between observed and modeled values of $<\eta>$ show no consistent dependence on season or chemical scheme. In most cases the difference between observed and modeled values of $|<\eta>|$ is no more than about 0.5, while the agreement between observed and modeled values of the phase of $<\eta>$, which is always poor, is significantly better for the four waves with the largest horizontal wavelengths. Some possible explanations to account for the differences between observed and modeled values of $<\eta>$ have been discussed, but their significance can only be assessed through careful numerical modeling.

For at least half of the observed waves, our modeled sets of $|<\eta>|$ values were within the observational errors. The comparatively large errors in the observed values of $|<\eta>|$ make it impossible to decide which chemical scheme used in the model provides the best results. The errors associated with the observed phases of $<\eta>$ are minimal, and cannot account for the differences between the observed and modeled phases of $<\eta>$.

Changing some of the values of the nominal chemistry-related parameters that are given in Table 1 did affect $<\eta>$, but not as significantly as those associated with varying season. Because of this, it is not possible to determine which chemical scheme performs best in our model.

Finally, although our model includes the effects of diffusion of heat and momentum in the gravity wave dynamics, these effects appear to be unimportant for most of the waves observed by *Zhang* [1991] and *Zhang et al.* [1992a]. Observations are required of waves having smaller spatial scales than can be resolved with the MORTI instrument in order to test our model-derived values of $<\eta>$ for waves affected by dissipation.

APPENDIX

Applying the production and loss terms provided in Table 2 to the undisturbed specie number densities, with $\overline{H}(M)=\overline{H}(O_2)=\overline{H}(N_2)$, gives us

$$\bar{n}\left[O_2\left(b^1\Sigma_g^+\right)\right] = \frac{\left\{e\bar{k}_1\bar{n}^2(O)\bar{n}(M)+\left[k_2\bar{n}(O_2)+\gamma k_3\bar{n}\left[O_2\left(c^1\Sigma_u^-\right)\right]\right]\right\}}{\left\{k_4\bar{n}(O)+k_5\bar{n}(N_2)+k_6\bar{n}(O_2)+A_2\right\}} \tag{A1}$$

where

$$\bar{n}\left[O_2\left(c^1\Sigma_u^-\right)\right] = \xi\bar{k}_1\bar{n}^2(O)\bar{n}(M)/\left\{k_2\bar{n}(O_2)+k_3\bar{n}(O)+A_1\right\}. \tag{A2}$$

The scale-heights of these species are

$$\overline{H}\left[O_2\left(c^1\Sigma_u^-\right)\right] = \left\{\frac{1}{\overline{H}(M)}\frac{\left[k_3\bar{n}(O)+A_1\right]}{\left[k_2\bar{n}(O_2)+k_3\bar{n}(O)+A_1\right]} + \frac{1}{\overline{H}(O)}\frac{\left[2k_2\bar{n}(O_2)+k_3\bar{n}(O)+2A_1\right]}{\left[k_2\bar{n}(O_2)+k_3\bar{n}(O)+A_1\right]}\right\}^{-1} \tag{A3}$$

and

$$\overline{H}\left[O_2\left(b^1\Sigma_g^+\right)\right]$$

$$= \left\{\frac{1}{H(M)}\left[1-\frac{\gamma k_3\overline{n}(O)}{D}\frac{\overline{n}\left[O_2\left(c^1\Sigma_u^-\right)\right]}{\overline{n}\left[O_2\left(b^1\Sigma_g^+\right)\right]}-\frac{\left[k_5\overline{n}(N_2)+k_6\overline{n}(O_2)\right]}{D}\right]\right.$$

$$+\frac{1}{\overline{H}(O)}\left[2-\left\{\left(2k_2\overline{n}(O_2)+\gamma k_3\overline{n}(O)\right)\frac{\overline{n}\left[O_2\left(c^1\Sigma_u^-\right)\right]}{\overline{n}\left[O_2\left(b^1\Sigma_g^+\right)\right]}+k_4\overline{n}(O)\right\}/D\right] \quad \text{(A4)}$$

$$\left.+\frac{\overline{n}\left[O_2\left(c^1\Sigma_u^-\right)\right]}{\overline{H}\left[O_2\left(c^1\Sigma_u^-\right)\right]}\left[k_2\overline{n}(O_2)+\gamma k_3\overline{n}(O_2)\right]\right\}^{-1}$$

where

$$D = k_4\overline{n}(O)+k_5\overline{n}(N_2)+K_6\overline{n}(O_2)+A_2 \ . \quad \text{(A5)}$$

Acknowledgments. This work was supported by NASA under contract NAS8-36639 (M.P.H.) and by the Aerospace Sponsored Research Program and NSF Grant ATM90-00216 (G.S. and R.L.W.). We are indebted to Susan Solomon, Rolando Garcia, and Helene LeTexier for supplying tabulations of output from the Garcia-Solomon model. We are grateful to the referees for their helpful comments.

The Editor thanks D. W. Tarasick and another referee for their assistance in evaluating this paper.

REFERENCES

Bates, D. R., Nightglow emissions from oxygen in the lower thermosphere, *Planet. Space Sci., 40*, 211, 1992.

Deans, A. J., G. G. Shepherd, and W. F. J. Evans, A rocket measurement of the $O_2\left(b^1\Sigma_g^+ - X^3\Sigma_g^-\right)$ atmospheric band nightglow altitude distribution, *Geophys. Res. Lett., 3*, 441, 1976.

Campbell, I. M., and C. N. Gray, Rate constant for $O(^3P)$ recombination and association with $N(^4S)$, *Chem. Phys. Lett., 18*, 607, 1973.

Chapman, S., Some phenomena in the upper atmosphere, *Proc. R. Soc. London, Ser. A, 132*, 353, 1931.

Garcia, R. R., and S. Solomon, The effects of breaking gravity waves on the dynamics and chemical composition of the mesosphere and lower thermosphere, *J. Geophys. Res., 90*, 3850, 1985.

Greer, R. G. H., E. J. Llewellyn, B. H. Solheim, and G. Witt, The excitation of $O_2\left(b^1\Sigma_g^+\right)$ in the nightglow, *Planet. Space Sci., 29*, 383, 1981.

Hickey, M. P., Effects of eddy viscosity and thermal conduction and Coriolis force in the dynamics of gravity wave driven fluctuations in the OH nightglow, *J. Geophys. Res., 93*, 4077, 1988a.

Hickey, M. P., Wavelength dependence of eddy dissipation and Coriolis force in the dynamics of gravity wave driven fluctuations in the OH nightglow, *J. Geophys. Res., 93*, 4089, 1988b.

Hickey, M. P., and K. D. Cole, A quartic dispersion equation for internal gravity waves in the thermosphere, *J. Atmos. Terr. Phys., 49*, 889, 1987.

Hickey, M. P., G. Schubert, and R. L. Walterscheid, Seasonal and latitudinal variations of gravity wave-driven fluctuations in OH nightglow, *J. Geophys. Res., 97*, 14, 911, 1992.

Hines, C. O., Internal gravity waves at ionospheric heights, *Can. J. Phys., 38*, 1441, 1960.

Hines, C. O., and D. W. Tarasick, On the detection and utilization of gravity waves in airglow studies, *Planet. Space Sci., 35*, 851, 1987.

Krassovsky, V. I., Infrasonic variations of OH emission in the upper atmosphere, *Ann. Geophys., 28*, 739, 1972.

Krupenie, P. H., The spectrum of molecular oxygen, *J. Phys. Chem. Ref. Data, I*, 423, 1972.

Martin, L. R., R. B. Cohen, and J. F. Schatz, Quenching of laser induced fluorescence of $O_2\left(b^1\Sigma_g^+\right)$ by O_2 and N_2, *Chem. Phys. Lett., 41*, 394, 1976.

Schubert, G., and R. L. Walterscheid, Wave-driven fluctuations in OH nightglow from an extended source region, *J. Geophys. Res., 93*, 9903, 1988.

Schubert, G., R. L. Walterscheid, and M. P. Hickey, Gravity wave-driven fluctuations in OH nightglow from an extended, dissipative emission region, *J. Geophys. Res., 96*, 13,869, 1991.

Slanger, T. G., Generation of $O_2\left(c^1\Sigma_u^-, C^3\Delta u, A^3\Sigma u^+\right)$ from oxygen atom recombination, *J. Chem. Phys., 69*, 4779, 1978.

Slanger, T. G., and G. Black, Interactions of $O_2\left(b^1\Sigma_g^+\right)$ with $O(^3P)$ and O_3, *J. Chem. Phys., 70*, 3434, 1979.

Solheim, B. H., and E. J. Llewellyn, An indirect mechanism for the production of $O(^1S)$ in the aurora, *Planet. Space Sci., 27*, 473, 1979.

Stegman, J., and D. P Murtagh, The molecular oxygen band systems in the *u.v.* nightglow: Measured and modelled, *Planet. Space Sci., 39*, 595, 1991.

Tarasick, D. W., and C. O. Hines, The observable effects of gravity waves on airglow emissions, *Planet. Space Sci., 38*, 1105, 1990.

Tarasick, D. W., and G. G. Shepherd, The effects of gravity waves on complex airglow chemistries 1, $O_2\left(b^1\Sigma_g^+\right)$ emission, *J. Geophys. Res., 97*, 3185, 1992a.

Tarasick, D. W., and G. G. Shepherd, The effects of gravity waves on complex airglow chemistries 2, OH emission, *J. Geophys. Res., 97*, 3195, 1992b.

Torr, M. R., D. G. Torr, and R. R. Laher, The O_2 atmospheric 0-0 band and related emissions at night from Spacelab 1, *J. Geophys. Res., 90*, 8525, 1985.

Viereck, R. A., and C. S. Deehr, On the interaction between gravity waves and the OH Meinel (6-2) and the O_2 atmospheric bands in the polar night airglow, *J. Geophys. Res., 94*, 5397, 1989.

Walterscheid, R. L., and G. Schubert, A dynamical-chemical model of tidally driven fluctuations in the OH nightglow, *J. Geophys. Res., 92*, 8775, 1987.

Walterscheid, R. L., and G. Schubert, Gravity wave fluxes of O_3 and OH at the nightside mesopause, *Geophys. Res. Lett., 16*, 719, 1989.

Walterscheid, R. L., G. Schubert, and J. M. Straus, A dynamical-chemical model of wave-driven fluctuations in the OH nightglow, *J. Geophys. Res., 92*, 1241, 1987.

Wiens, R. H., S.-P. Zhang, R. N. Peterson, and G. G. Shepherd, MORTI: A mesopause oxygen rotational temperature imager, *Planet. Space Sci., 39*, 1363, 1991.

Zhang, S., Gravity waves from O_2 airglow, Ph.D. dissertation, York University, Ontario, Canada, Sept. 1991.

Zhang, S., R. N. Peterson, R. H. Wiens, and G. G. Shepherd, Gravity waves from O_2 nightglow during the AIDA '89 Campaign, I, Emission rate/temperature observations, *J. Atmos. Terr. Phys.*, 355, 1992a.

Zhang, S., R. H. Wiens, and G. G. Shepherd, Gravity waves from O_2 nightglow during the AIDA '89 Campaign, II, Numerical modeling of the emission rate/temperature ratio, η, *J. Atmos. Terr. Phys.*, 377, 1992b.

M. P. Hickey, Physitron, Inc., 3304 Westmill Drive, Huntsville, AL 35805.

G. Schubert, Department of Earth and Space Sciences and Institude of Geophysics and Planetary Physics, University of California, Los Angeles, CA 90024.

R. L. Walterschied, Space and Environment Technology Center, The Aerospace Corporation, Los Angeles, CA 90009.

(Received May 13, 1992;
revised September 25, 1992;
accepted September 25, 1992.)